

# Additive Influence on Binder Migration in Electrode Drying

David Burger,\* Julian Klemens, Noah Keim, Marcus Müller, Werner Bauer, Joyce Schmatz, Jana Kumberg, Philip Scharfer, and Wilhelm Schabel

Two main goals for the industrial, slurry-based electrode processing are a high process speed and the maximum possible material efficiency. This makes an increased drying rate and active material share favorable, but both are limited by adverse effects on the electrode quality. The adverse effects of fast drying are associated with the migration of binder. In this article, the slurry properties of water-based graphite slurries are manipulated using a synthetic, layered silicate as additive. The influence of the polymer-particle composite network on the viscosity, adhesion strength, and cell performance is investigated. By addition of a small amount of additive (0.5 wt% of the dry electrode), the binder migration is mitigated up to a drying rate of  $6 \text{ g m}^{-2} \text{ s}^{-1}$  for graphite anodes with  $\approx 4.2 \text{ mAh cm}^{-2}$  (corresponding with 30 s drying time) leading to a possible increase of eight times the process speed compared to drying with  $0.75 \text{ g m}^{-2} \text{ s}^{-1}$  if adverse effects on the tortuosity of the electrodes can be solved. In this work, a combination of additive usage is pointed out with a multilayer approach and first insights are provided in how the binder migration may be mitigated to gain structurally optimized fast-dried electrodes without losses in electrode quality.

## 1. Introduction

For slurry-based battery electrodes, the drying rate during the formation of the porous microstructure is one of the key limiting factors for a higher processing speed. With increasing drying rate, the electrochemical and mechanical properties are both adversely affected.<sup>[1–7]</sup> An accumulation of binder in pores and on the active materials' surfaces in the top region of the electrode

leads to an increase of ionic resistance and affects both cycle stability and C-rate capability. Among the drying rate, the influence of numerous other process parameters like the areal mass loading, the properties and content of thickener, and the distinct influence of an increase in drying rate by temperature or heat-transfer coefficient are discussed in literature,<sup>[4,8,9]</sup> but a fundamental understanding of the binder migration is still pending.

The phenomenon of binder or particle migration is widespread in drying of suspensions.<sup>[10,11]</sup> Mechanistic understanding of the underlying effects is given, e.g., by Luo et al.<sup>[10]</sup> who propose a combination of top-down consolidation process and capillary transport after microstructure formation.<sup>[10]</sup> These concepts were shown to be partially applicable to battery electrode coatings, where capillary transport, acting at latest after the end of the film shrinkage,

is thought of to be mainly responsible for the migration of binder (see Section 1.1).<sup>[12,13]</sup>

Various sources exist that show the influences of binder migration on cell performance,<sup>[1–3,6]</sup> or investigate the microstructure by energy-dispersive X-Ray spectroscopy (EDS) or other spectroscopic methods.<sup>[2,12]</sup> In correlation with the binder distribution or the electrochemical performance, the decrease of adhesion strength with increasing drying rate has been proven to be an accessible indicator for binder migration.<sup>[3–5]</sup>

Beyond electrodes processed with *N*-methyl-2-pyrrolidone (NMP) as solvent and polyvinylidene fluoride (PVDF) as binder, especially for electrodes with water-based slurries, containing the dispersed latex binder styrene-butadiene rubber (SBR) and the dissolved thickener carboxymethyl cellulose (CMC), the level of complexity is higher as both components can migrate. Here, a reduced binder migration was reported to be achievable by changes of the particle properties due to intensive mixing procedures<sup>[1,14]</sup> or directly by choosing an active material with different size and/or surface chemistry.<sup>[1,15,16]</sup>

However, coatings based on the CMC/SBR system are no technology limited to battery electrodes. In literature, the formation of stable polymer-particle networks of CMC, SBR, and other particles is associated with the mitigation of binder migration for processes in the field of paper coating.<sup>[17,18]</sup> For these systems, it is indicated that the film formation process and fixation of SBR is affected by the type of SBR-latex, its glass-transition temperature, mass fraction, and the molecular weight and degree of substitution of thickener or co-binder CMC.<sup>[18]</sup>

D. Burger, J. Klemens, J. Kumberg, P. Scharfer, W. Schabel  
Thin Film Technology (TFT)  
Karlsruhe Institute of Technology (KIT)  
Straße am Forum 7, D-76131 Karlsruhe, Germany  
E-mail: david.burger@kit.edu

N. Keim, M. Müller, W. Bauer  
Institute for Applied Materials (IAM) – Energy Storage Systems (ESS)  
Karlsruhe Institute of Technology (KIT)  
Hermann-von-Helmholtz-Platz 1, D-76144 Eggenstein-Leopoldshafen,  
Germany

J. Schmatz  
MaP – Microstructure and Pores GmbH  
Junkerstraße 93, D-52064 Aachen, Germany

 The ORCID identification number(s) for the author(s) of this article can be found under <https://doi.org/10.1002/ente.202400057>.

© 2024 The Authors. Energy Technology published by Wiley-VCH GmbH. This is an open access article under the terms of the Creative Commons Attribution License, which permits use, distribution and reproduction in any medium, provided the original work is properly cited.

DOI: 10.1002/ente.202400057

### 1.1. Characteristics of Binder Migration for a CMC/SBR Binder System

To understand the influence of material properties on the binder migration behavior, the literature presented earlier is connected to the drying mechanism in more detail:

During drying, the concentrations of CMC, SBR, and other particles rise and the distances between particles decrease constantly. The film shrinkage, based on diffusive solvent transport, is mostly uniform for moderate drying rates. It terminates at latest when the particles, mainly active material, come into contact, constituting a porous network filled with a polymer solution that contains dispersed SBR and carbon black (CB). If the drying rate is high enough, a gradient in solvent concentration may built up during the film shrinkage, as shown for the drying of NMP-based graphite anodes by Jaiser et al.<sup>[12]</sup> with a drying rate of  $1.2 \text{ g m}^{-2} \text{ s}^{-1}$  as well as for drying CMC films by Eser et al.<sup>[19]</sup> with even lower drying rate (LDR).

After the formation of a saturated pore network and hence the ability to form menisci, the solvent volume is further reduced by drying, leading to the emptying of pores in sequence of their pore diameter. Driven by capillary action, smaller pores remain filled. A superposition of capillary-induced convection and diffusional solvent transport maintains the solvent transport to the electrode surface. Both maintain the drying rate. When the liquid retreats into the pores, a share of the SBR and CMC binder migrates, respectively,<sup>[13,17]</sup> with the solvent toward the phase interface where evaporation is taking place. During drying, fixed parts of binder and the conductive additive remain in the interstices among the particle contact points of the pore network. For CB, it is shown in literature that the migration is dependent on the thickness of the electrodes and does not occur significantly for moderate areal mass loadings.<sup>[2]</sup> However, for sequentially processed multilayers, movement of CB by capillary transport can play a role.<sup>[20]</sup>

The understanding of the drying process led to different strategies to overcome the negative influence of binder migration: The application of a multilayer structure containing differently sized particles with different morphology shown by Kumberg et al.<sup>[1]</sup> can be an appropriate approach to change the sequence of pore emptying, mitigating the built-up of a saturation gradient over the full height of the cross section because smaller pores remain filled preferably. Another possibility, limited to a system of separated components as thickener and binder (like for CMC/SBR), is the grading of the SBR-binder content in a multilayer structure that is intended to balance the influence of binder migration on the distribution of SBR.<sup>[21]</sup>

From literature, it is known that the binder migration ends after a certain point in the drying process. From the possible mechanisms to end the relevant interval for the migration, two are highlighted here: migration of SBR may cease either when the saturation of the pore network becomes insufficient to sustain migration through a connected capillary network,<sup>[3]</sup> or when the polymer matrix initially or eventually fixes the binder in place during the drying process as it contracts. In the case of CMC, entanglement is expected to occur below a certain concentration limit.<sup>[22,23]</sup> Regarding the latter, sources from the field of paper coating indicate that the achievement of a “gel-point”

during drying leads to an immobilization of dispersed SBR in a CMC matrix between the particles of the coating.<sup>[18,24,25]</sup>

### 1.2. Additive Usage

A possible approach to manipulate the formation of composite networks and colloidal gels is the use of additives. Promising for the use in water-based battery electrode slurries is the additive LAPONITE®. Investigated for CMC and polyacrylic acid (PAA) as co-binders, it shows a positive impact on the electrochemical performance and adhesion.<sup>[26,27]</sup>

LAPONITE® is a synthetic-layered silicate and finds application as an additive in several fields of product design.<sup>[28–30]</sup> The synthetic clay can be dispersed as single flat discs in water and gets partially polarized at face and edge surfaces with different charges due to its crystalline structure. Thus, it is able to build an electro-steric network with itself or by interaction with other slurry components, leading to a shear-thinning, thixotropic flow behavior.<sup>[31,32]</sup> The reason for gel-like behavior of LAPONITE® in water is the formation of a network mainly dependent on edge-face interactions between the plates.<sup>[33,34]</sup> It differs from the structure of gel-like polymer solutions. LAPONITE® can form polymer–particle networks with CMC. As the dimensions of CMC (0.5 nm per glucose unit<sup>[35,36]</sup>) must be, in any configuration, several times bigger than the size of a  $\approx 25 \text{ nm}$  LAPONITE® plate, an interconnected network can be formed, with gel-like behavior even below the concentrations one would expect for the single components.<sup>[34,37,38]</sup> This means that one CMC chain can interact with several LAPONITE® plates either by interaction between the negatively charged groups of the anionic polyelectrolyte CMC and the pH-dependent positively charged sides of the LAPONITE® plates<sup>[32,34]</sup> or by hydrogen bonding to the faces of the plate.<sup>[30,37]</sup> The magnitude of the synergistic effect is specific for CMC and LAPONITE®, as shown by Fitch et al. comparing the mixture with blends of hydroxyethyl-cellulose, xanthan gum, and PAA, respectively.<sup>[34]</sup>

In this work, the impact of slurry properties on the binder migration behavior is investigated by comparison of the shear behavior and microstructure of different slurry compositions with the behavior of the adhesion strength at increasing drying rate. Purposefully manipulated slurry properties are linked with the investigation of the mechanical and morphological properties of the dry electrodes regarding binder migration. Further, LAPONITE® is traced by EDS as a measure for the component distribution over the height of the electrode. The measurement technique is used to investigate the migration of components in electrodes with multilayer architecture.

## 2. Results and Discussion

To possibly reduce the manufacturing time while achieving the highest material efficiency, the drying of additive-supported slurries is investigated. The addition of the additive is intended to reduce the mobile fraction of the SBR binder and mitigate the binder migration at high drying rates. In addition, a reduction of passive materials (CMC/SBR and CB) is aimed to obtain the highest possible share of active material in the electrodes.

To reach this, the use of an additive LAPONITE® in several formulations is investigated along the process chain.

## 2.1. Impact of Additive Content on Slurry Viscosity

The two-substance system of CMC and LAPONITE® in water is characterized by shear rheometry. The objective is to show the interaction of the additive and CMC in the polymer–particle network built up in water-based CMC/SBR electrode slurries. **Figure 1** shows the viscosity of a CMC solution (2 wt% in water) compared to a CMC-additive dispersion (2 wt%/0.5 wt% in water) and additive dispersion (0.5 wt% in water) for increasing shear rate among the classification into gel-like and liquid-like behavior by means of the storage and loss modulus for increasing frequency.

All three fluids show a shear-thinning behavior. Apparent is the influence of the 0.5 wt% additive on the low-shear viscosity at  $0.01 \text{ s}^{-1}$ . The value of  $13.7 \pm 1.8 \text{ Pa s}$  is shifted by two orders of magnitude to a value of  $5970 \pm 1020 \text{ Pa s}$ . The increase is not caused by the interaction of the additive with itself, which builds a network disruptable by shear (Figure 1, additive). Moreover, it is evoked by interactions between the polymer chains functional groups and the differently polarized surfaces of the additive, forming a polymer–particle composite. The behavior is typical for CMC–LAPONITE® mixtures in water according to literature.<sup>[32,34,37]</sup> Besides influencing the shear viscosity, the interaction leads, for the given deformation, to a gel-like (phase angle  $<45^\circ$ ) behavior of the CMC-additive dispersion compared to a liquid-like (phase angle  $>45^\circ$ ) behavior of the CMC solution.

Indicator for the structural strength of the polymer–particle network is the high, constant storage modulus in case of the CMC-additive dispersion.<sup>[39,40]</sup> The flow behavior indicates that the CMC chains interact on a molecular level with the clay plates to form a 3D interconnected network, that is disrupted by shear, but capable of being reformed reversibly. Such a network may provide the opportunity to contain also other components in it like SBR in a water-based battery slurry.

The slurries for the anodes were prepared, so that the dry electrodes have the composition given in **Table 1**, with and without the additive LAPONITE®.

**Figure 2** shows the viscosity of the slurries “Reference,” “A100” (with additive, 100% of passive materials), “A75,” and “A66” (with additive, passive material reduced by 25% and 33%, respectively) versus the shear rate among with the oscillatory measurement.

A gel-like behavior is found not only in the CMC-additive dispersion but in all battery slurries containing the additive (A100, A75, and A66). Compared to the Reference that shows a clear liquid-like behavior with an average phase angle of  $66^\circ \pm 3^\circ$ , over the entire frequency range (like the same slurry composition in the literature<sup>[1]</sup>), the inter-particle and intermolecular interactions in the slurries containing the additive induce a gel-like behavior (phase angle  $<45^\circ$ ) and elevate the low-shear viscosity for all the investigated compositions. The stability of the colloid network is shown by an almost constant storage modulus over the frequency range. In case of A66, a transition toward a liquid-like behavior is conceivable. The higher the concentration of the passive materials and additive are chosen, the stronger is

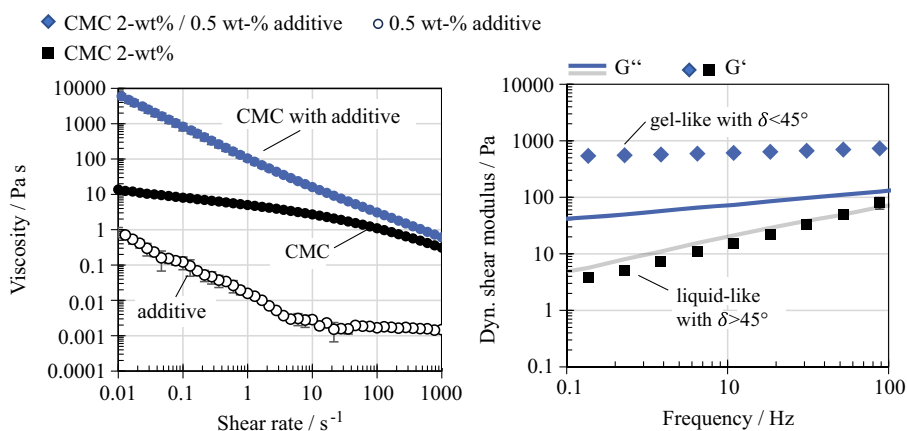


**Figure 1.** Left: viscosity of a 2 wt% CMC solution compared to a 2 wt%/0.5 wt% CMC-additive dispersion and a dispersion of 0.5 wt% additive in water versus the shear rate. Right: storage and loss modulus for an oscillatory measurement versus the frequency at a deformation of 1%. The phase angle  $\tan(\delta) = G''/G'$  (Section S1, Supporting Information) is used as criterion for gel- or liquid-like behavior.

**Table 1.** Composition of dry electrodes. For all slurries, the solids have a mass fraction of 43 wt%.

Name	Active			Passive		Passives compared to A100
	Graphite [wt%]	CB [wt%]	CMC [wt%]	SBR [wt%]	Additive [wt%]	
Reference (Ref.)	93.00	1.40	1.87	3.73	–	–
A100	92.50	1.40	1.87	3.73	0.50	100%
A75	94.40	1.05	1.40	2.80	0.35	75%
A66	95.00	0.94	1.25	2.45	0.31	66%

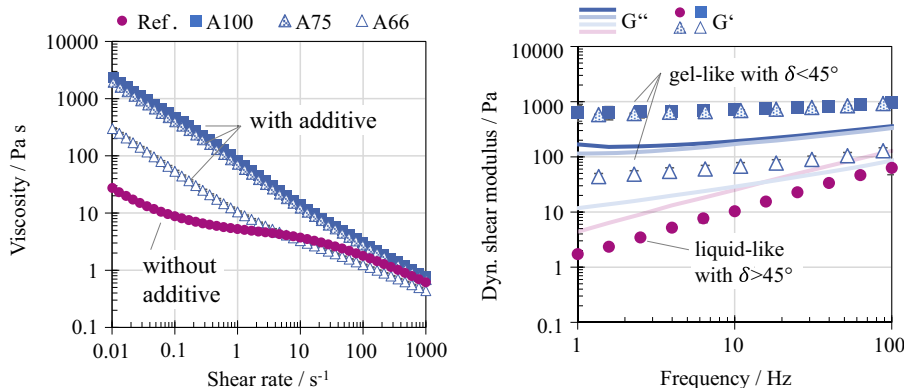


**Figure 2.** Left: viscosity of the slurries Reference, A100, A75, and A66 versus the shear rate. Right: storage and loss modulus versus the frequency for a deformation of 1%. The phase angle  $\tan(\delta) = G''/G'$  (Section S1, Supporting Information) is used as criterion for gel- or liquid-like behavior.

the shift toward a network-stabilized slurry. Also, at high shear rates (interaction between additive and CMC mostly broken down), the concentration of passive materials (CMC and CB concentration) determines the viscosity. This leads to a lower viscosity at  $1000 \text{ s}^{-1}$  for A66 compared to the Reference. A gel-like behavior may also be induced by a higher concentration of CMC, however at a undesirably higher concentration depending on the properties of the CMC.<sup>[22,41]</sup>

The strong shear-thinning behavior with a viscosity below  $10 \text{ Pa s}$  in the coating-relevant range of shear rate makes it feasible for all the slurries to be coated by knife coating or, as state-of-the-art coating technology in battery processing by slot-die coating.<sup>[42]</sup> However, agitation of the slurry A100 to be pumped may be a challenge.

In addition to interactions between additive and polymer, the question arises if there is a grinding of particles during mixing due to the increased energy input following with the higher viscosity of the slurry A100. This cannot be confirmed by the particle size distribution (Section S2, Supporting Information). Thus, no influence of a change in the active material particles on the microstructure is expected, allowing conclusions to be drawn about the influence of passives and the additive on the microstructure formation and binder migration.

## 2.2. Adhesion Strength

A decrease of the adhesion strength of electrodes for increasing drying rate has been shown to be an indicator for the formation of an inhomogeneous microstructure by binder migration.<sup>[3–5,16]</sup> In Figure 3 and 4, the adhesion strength of electrodes made with the slurries Reference, A100 (with additive, 100% of passive materials), A75, and A66 (with additive, passive material reduced by 25% and 33%) is compared for increasing drying rate, respectively. To investigate the applicability for a multilayer structure as well, the adhesion strength of a simultaneously coated multilayer electrode with a thickness ratio of 1:1 with the slurry Reference coated over A100 is shown in Figure 4. The slurries have the same solid content of 43 wt% and all electrodes have the same coating weight of  $121 \pm 6 \text{ g m}^{-2}$ , a dry film thickness of  $139 \pm 7 \mu\text{m}$ , and a porosity of  $58 \pm 2\%$ . For detailed information, please see Section S3 and S4, Supporting Information.

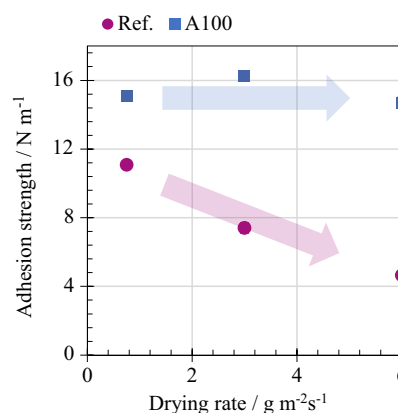


**Figure 3.** Adhesion strength of electrodes made with the slurries Reference and A100 with the same SBR-binder content for increasing drying rate. The slurries have the same solid content of 43 wt% and the electrodes the same coating weight of  $121 \pm 6 \text{ g m}^{-2}$ , a film thickness of  $139 \pm 7 \mu\text{m}$ , and porosity of  $58 \pm 2\%$ .

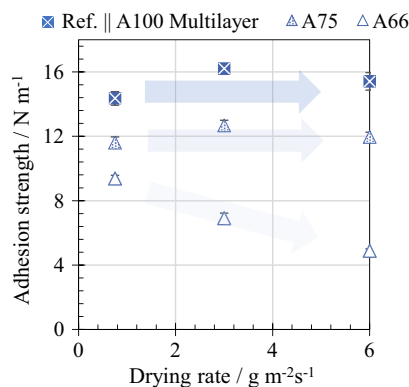


**Figure 4.** Adhesion strength of electrodes made with the slurries A75 and A66 with a reduced binder and additive content (by 25% and 33%, respectively) among a multilayer with thickness ratio 1:1 with Reference simultaneously coated over A100 for increasing drying rate. The slurries have the same solid content of 43 wt% and the electrodes have the same coating weight of  $121 \pm 6 \text{ g m}^{-2}$ , a film thickness of  $139 \pm 7 \mu\text{m}$ , and porosity of  $58 \pm 2\%$ .

The electrodes made with the Reference slurry show the expected behavior of a decreasing adhesion strength with increasing drying rate. The values reproduce the trend in published measurements by Kumberg et al. obtained with the same experimental setup, materials, and mass fractions as in this work.<sup>[1,4]</sup> For the electrodes made with the slurries A100 and A75 (both with additive), the adhesion strength is not dependent on the drying rate inside the investigated drying-rate range. The increase in drying rate corresponds to a reduction of drying time from over 3 min to only 30 s. For an industrial dryer with a fixed length of 50 m for single-side drying, this would lead potentially to an increase in manufacturing speed from 15 to over 100 m min<sup>-1</sup>, which is including the process speed range for a state-of-the-art industrial process.<sup>[43]</sup>

The adhesion strength of A75 is with an average value of 12.1 Nm<sup>-1</sup> by 21% reduced compared to 15.3 Nm<sup>-1</sup> of A100, which resembles the reduction of the passive material. A further reduction for A66 leads to an adhesion strength of 9.3 Nm<sup>-1</sup> for the lowest drying rate, which follows an almost linear relationship between binder content and adhesion strength in accordance to Diehm et al. for a change of just the mass fraction of SBR.<sup>[21]</sup> Hofmann et al. could confirm an increase of adhesion strength with increasing SBR mass fraction with negative effect of increasing SBR mass fraction on the cell performance.<sup>[44]</sup> In contrast to A100 and A75, the adhesion strength of the electrodes made with the slurry A66 is deteriorating with increasing drying rate like for the Reference. Although there is 33% less SBR, CMC, and CB present in the dry electrode, the adhesion strength is comparable to the Reference electrode. The addition of LAPONITE® leads presumably to an increase in adhesion strength.

As a contrary result to the single-layer Reference, the multi-layer electrode (Ref. || A100), with additive in the slurry A100 only in the substrate-near half of the electrode shows an adhesion strength comparable to the single layer made with A100, even with increasing drying rate. The samples in the peel test showed clean delamination of the electrode from the current collector, no different than the single layers (no delamination between layers). According to the results it may only be necessary for the substrate-near layer to supply a strong fixation of SBR against migration to dominate the adhesion to the current collector. However, binder migration in the upper layer itself is still possible even if the adhesion strength as local measurement remains unchanged with increasing drying rate. If there is a migration happening is further discussed in **Section 2.3**. According to literature on the connection between slurry microstructure and binder migration, one could get the impression that a gel-like slurry tends to show a mitigated migration behavior. Significantly reduced binder migration has been shown for the drying of graphite anode slurries mixed with a kneader or hard carbon with smaller particle size.<sup>[1,16]</sup> Slurries with smaller particles show a shift toward a gel-like behavior, indicating more interactions between the components. It is to be noticed that the slurry A66 still shows a gel-like behavior (phase angle <45°), however, with frequency-dependent storage modulus. The network may not be as stable as in case of A100 and A75. This indicates that a network, detected by oscillatory shear rheology, only suggests a mitigated binder migration with increasing drying rate, but it cannot predict it. Klemens et al. showed similar results

for the comparison of hard carbon electrodes of differently sized hard carbon for increasing drying rate.<sup>[16]</sup> In their work, a slurry with liquid-like behavior showed no binder migration up to a drying rate of 3 gm<sup>-2</sup> s<sup>-1</sup>, but then changed into migration behavior for a further increase in drying rate. Other but smaller sized hard carbons showed a gel-like behavior of the slurry and no binder migration. They hypothesized that the onset of binder migration for increasing drying rate is determined by the fixation of the “CMC network” (CMC/SBR and CB), which can be disturbed by disruptive capillary transport at a high drying rate. According to this, the higher adhesion strength in case of additive usage indicates a mitigated binder migration that could originate from a changed microstructure of the polymer-particle network. To not only increase the adhesion strength but mitigate the binder migration effectively a concentration limit between A75 and A66 must be reached as indicated by the transition toward a loss of adhesion strength with increasing drying rate for the slurry from A75 to A66.

It must be noted that the same increase in drying rate by changing the flow conditions other than increasing the drying temperature (as investigated in this work) may show a decrease of adhesion strength, as shown in literature for anodes using CMC/SBR as binder.<sup>[4,16]</sup>

## 2.3. Binder Distribution

### 2.3.1. Microstructure in the Wet State

To assess the influence of a changed fixation of the binder and obtain a better understanding of the adhesion-strength measurements, SEM images of the slurry as well as of the dry microstructure can be used. One method to reveal the structure of the colloid network, especially in a slurry with particulate binder, is cryo-SEM.<sup>[1,17,22,45]</sup> The method has been used to compare slurry microstructures and the distribution of CMC/SBR/CB and active material.<sup>[1,22]</sup> By freezing the slurry with a nitrogen slush and preparing a cross section under liquid nitrogen, it is possible to take SEM images of the slurry microstructure. In addition to the shape of the graphite particles and its general arrangement, the cryo-SEM technique also shows the surfaces of the active material particles and a freeze-out structure, which is partially influenced by plunge freezing of the water.<sup>[1,12,45]</sup> Freeze-outs refer to the porous structure of the composite network that remains after sublimation of the water between the active material particles. The experimental procedure of Kumberg et al.<sup>[1]</sup> was used to investigate the microstructure of the slurry A100 in comparison to the slurry Reference, having the same composition and mixing routine as in the literature. **Figure 5** (first row) shows the general arrangement of the components for A100 and the Reference.

The image of the slurry A100 shows that the size and shape of the active material is almost identical to the Reference, which confirms the measurements for the particle size (Section S2, Supporting Information). However, the composite network between the particles consisting of CMC/SBR and CB differs. The freeze-out bridges connecting the particles seem to be wider and of a bigger diameter in case of A100 compared to the dispersed freeze-outs with a thinner and more ramified structure in case of the Reference. **Figure 5** (second row) shows a higher

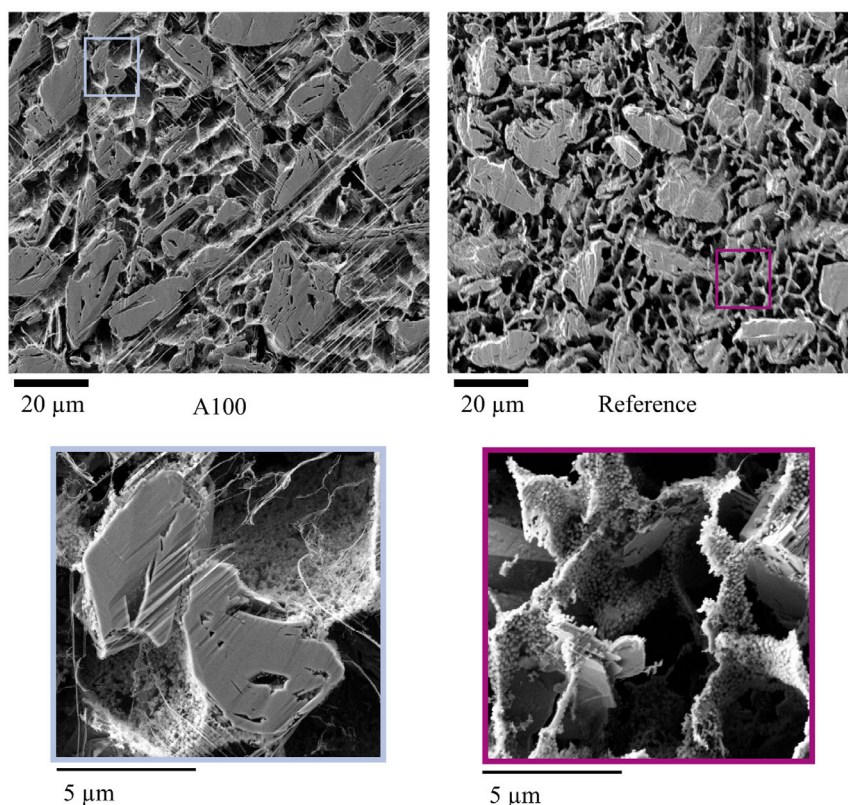


**Figure 5.** Left: Cryo-SEM image of the slurry A100. Right: Cryo-SEM image of the slurry Reference. The slurries have the same composition and the same mixing procedure in addition to the addition of LAPONITE<sup>®</sup> to A100. It is to be noted that the filamentary structures in the image of A100 are artifacts of the broad ion beam treatment. Regions for magnification are marked, respectively. CMC, CB, and SBR form a composite network with freeze outs covered with SBR. For more and full-size images of the details, see Section S5, Supporting Information.

magnification of the contact between the graphite and the other materials (for more and full-size images of the details see Section S5, Supporting Information).

In both cases, the surface of the freeze-outs in the composite network is populated by SBR, like shown in literature for the Reference [1]. The authors would like to point out that the further description is based on subjective impression: A close look on the freeze-out surfaces reveals that they are more homogeneously and densely populated by SBR for the slurry A100. Thus, the contact points to particles and the bridges between them are covered more by SBR binder.

From cryo-SEM investigations by Lim et al. it is known that CMC would competitively adsorb on graphite, hindering the SBR adsorption on the graphite which is then dispersed in a colloid network between the graphite.<sup>[22]</sup> As SBR particles are generally made polar in water-based dispersions by the use of surfactants<sup>[46]</sup> or using carboxylated SBR,<sup>[47]</sup> the SBR particles may be attracted to the charged surface of the additive LAPONITE<sup>®</sup>. Considering the interaction between CMC and the additive, this could form a stable composite network. Among the structure of the colloid network, also its contact with the graphite might be changed, depending on the surface structure of the graphite.<sup>[48]</sup> This behavior could be shown by comparison of graphite with different surface chemistry by Kumberg et al.<sup>[1]</sup> and Chang et al.<sup>[17]</sup> with focus on the shape of the contact

between the particles and the composite network. Other sources report that the adsorption behavior of CMC on graphite is strongly influenced by the presence of impurities as centers for adsorption,<sup>[49]</sup> that may be augmented by adsorbed LAPONITE<sup>®</sup> on the graphite surface. From literature, it is known that LAPONITE<sup>®</sup> is able to adsorb on a variety of particles including carbon nanotubes<sup>[50]</sup> and also graphite<sup>[51]</sup> itself.<sup>[51]</sup> Although not to be quantified, a comparison of different concentrations of LAPONITE<sup>®</sup> and graphite shows that it works as dispersing agent (Section S6, Supporting Information), which suggests adsorption of the additive on the graphite surface. With the same graphite used for both slurries, the additive may act as an intermediary between the surfaces of the hydrophobic graphite and the CMC-composite network.

From this point, it is unclear which exact interaction between slurry components and the additive is the cause for the mitigated binder migration. However, a general finding can be made: a changed behavior of the composite network leads to fixation of the SBR during capillary transport.

To further investigate this, a characterization by means of zeta-potential measurements<sup>[50,52–55]</sup> may help to understand the interactions between the components better and answer the question if LAPONITE<sup>®</sup> is an intermediary between CMC-composite network and the graphite surface or mainly interacts with the CMC to form a stable network during drying.

### 2.3.2. Microstructure in the Dry State

The results of the adhesion strength measurements indicate that much less binder migration is happening for the electrodes made with A100 and a multilayer structure with A100 in the bottom layer and the Reference in the top layer. A dominating effect of the bottom layer on adhesion has also been shown for binder-graded, multilayer electrodes by Diehm et al.<sup>[21]</sup> concentrating the amount of SBR in the lower layer of the electrode. One objective of this was a changed, at least even, distribution of the binder after drying. However, this was not possible to be directly shown experimentally. EDS, commonly used for visualization of the components' distribution in battery electrodes with an NMP–PVDF solvent-binder system,<sup>[3,5,6]</sup> is unable to differ SBR from CMC and CB. As the LAPONITE®, containing Mg and Si, holds atoms specific for it, it is among an additive also a tracer substance. By comparing the initial composition and the composition of the dry electrode, findings about the migration of components in water-based multilayer electrodes can be derived. This holds especially for the case of a multilayer with no LAPONITE® in the upper layer.

Figure 6 shows the mass fraction of magnesium (Mg) and silicon (Si) specific for the additive as well as for sodium (Na) present in CMC and the additive derived from EDS of the top surface of the electrodes made with A100, A66, and the multilayer Ref. || A100 dried with a drying rate of  $3 \text{ gm}^{-2} \text{ s}^{-1}$ .

The results show an average decrease of 37% in the signal of Na, Mg, and Si from A100 to A66. This matches with the theoretical decrease by a reduction of the additive amount by 33%. As the additive can be identified by its specific Mg and Si signals, it should be detectable at the top surface in case of migration during drying. However, for the investigation of the multilayer electrode Ref. || A100, no Mg and Si was detected at the top surface.

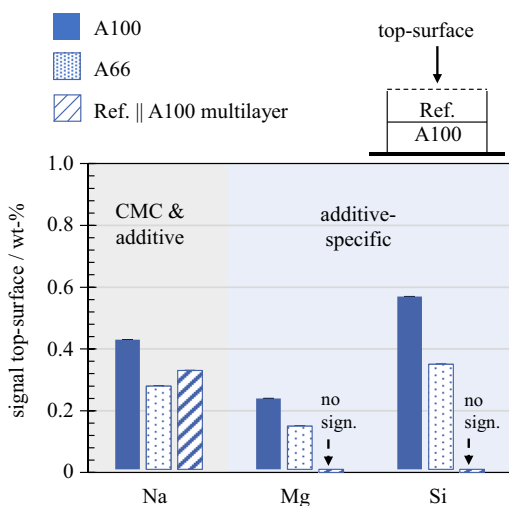


**Figure 6.** Mass fraction (wt%) of Na (CMC and additive), Mg and Si (additive specific) from EDS of the top surface of the electrodes made with the slurries A100, A66, and a multilayer of thickness ratio 1:1 with Reference coated simultaneously over A100. The electrodes were dried with the same drying rate of  $3 \text{ gm}^{-2} \text{ s}^{-1}$ . For the multilayer, no migration of the additive from the bottom layer to the top of the electrode can be observed (no sign.).

This shows that a migration of the additive is, for the multilayer, not taking place from out the bottom layer. Capillary action is not able to transport a significant amount of additive from the middle of the electrode (where the layers are coated on each other) toward the top surface, although capillary transport and binder migration especially in the upper layer itself were suspected.

At this point, it is known that the microstructure of the slurry, the microstructure formation and the microstructure in the dry state are influenced by the additive.

### 2.4. Electrochemical Characterization

For more binder migration present at higher drying rate (HDR), the C-rate capability is adversely affected due to an increased ionic resistance.<sup>[2,3,6]</sup> In the following, it will be investigated if the structural changes by the binder migration mitigating additive are beneficial for electrochemical performance or must be contained in a functional layer. To test applicability of the additive in a battery electrode, full cell tests were conducted. Possible changes regarding the drying rate are considered by comparison of an LDR ( $0.75 \text{ gm}^{-2} \text{ s}^{-1}$ ) and HDR ( $6 \text{ gm}^{-2} \text{ s}^{-1}$ ), respectively.

Figure 7 shows the specific discharge capacity ( $\text{mAh g}^{-1}$  of NCM622) for an increasing C-rate cycling protocol with a subsequent test for cycle stability (Section S8, Supporting Information) for the electrodes made with the slurries Reference and A100 at LDR and HDR.

All cells show a comparable specific discharge capacity of  $166.8 \pm 0.8 \text{ mAh g}^{-1}$ , which shows that the additive is mostly chemically inert and does not adversely affect the formation process. Information about the voltage profile of the initial cycles can be found in the Section S7, Supporting Information. In addition, it should be noted that long-term cycling shows that there are no side reactions that reduce capacity in the long term, as can be seen in Section S8, Supporting Information. As the C rate is increased from 1 to 3 C, major differences evolve between the faster and slower dried electrodes made with the slurry Reference. The specific capacity of the cells with the faster dried anode Reference drops 10% more from C/20 to 1 C and from

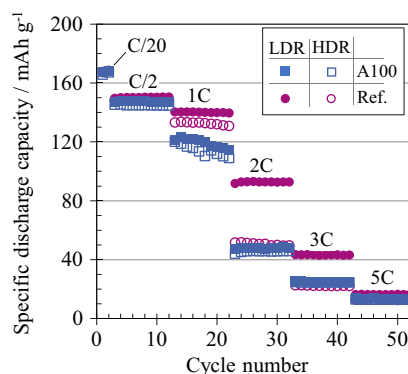


**Figure 7.** Specific discharge capacity ( $\text{mAh g}^{-1}$  of NCM622) for full cells with anodes made with the slurries Reference and A100 for the lower drying rate (LDR) of  $0.75 \text{ gm}^{-2} \text{ s}^{-1}$  and the higher drying rate (HDR) of  $6 \text{ gm}^{-2} \text{ s}^{-1}$ , respectively. The standard deviation between three separate measurements is less than 10% of the specific discharge capacity, respectively, and is not shown for clear form of presentation.

C/20 to 2 C even 56% more. This behavior can be explained by an increased ionic resistance due to an accumulation of SBR at the top of the electrode. The cells with the anode A100 do not show the same trend for increasing drying rate. Both slower and faster dried A100 anodes exhibit a decrease in specific capacity compared to the Reference. Specifically, the capacity drops by 20% when transitioning from C/20 to 1 C, and by 60% when transitioning from C/20 to 3 C. For 3 and 5 C, the fast dried anodes made with Reference and A100 behave equally, as the diffusion limitation in the cathode becomes the determining factor for specific discharge capacity at high C rates. For the long-term cycling at 1 C, the effects of drying and additive remain. However, the C-rate capability of A100 is worse than the Reference at 1 and 2 C. This may be attributed to a change in ionic resistance due to a change in the electrodes microstructure.

To determine the origin of the changed C-rate capability for the A100 anodes, the ionic resistance  $R_{ion}$  is evaluated using electronic impedance spectroscopy (EIS).<sup>[57]</sup> Landesfeind et al. assert that  $R_{ion}$  is a part of the impedance that scales with changes of the transport path  $L$ , porous cross section  $A\epsilon$  (with the average porosity  $\epsilon$ ) but also with local changes in the microstructure (Equation (1)).<sup>[57]</sup> The ionic resistance can be transferred into an effective tortuosity  $\tau_{eff}$ , which is not interchangeable with other tortuosity definitions like e.g., the path-length tortuosity  $\tau_{path} = L_{eff}/L$ .<sup>[57]</sup> The primary advantage of  $\tau_{eff}$  over  $R_{ion}$  lies in the comparability of different electrode samples, which may have deviating thickness, porosity and cross section, concerning changes in their microstructure by, e.g., binder migration.<sup>[6]</sup>

$$R_{ion} \propto \frac{L_{eff}}{A\epsilon} = \frac{L}{A} \frac{\tau_{eff}}{\epsilon} \text{ with } \tau_{eff} \neq \tau_{path} \quad (1)$$

Figure 8 shows the effective tortuosity of the electrodes made with Reference and A100 for the drying rates LDR and HDR.

On the one hand, the effective tortuosity of the electrodes made with the slurry Reference portray the effect of binder migration on the effective tortuosity of electrodes by a rise of 80% from drying with LDR to HDR. An accumulation of binder may lead here to longer pathways and decreased cross-sectional

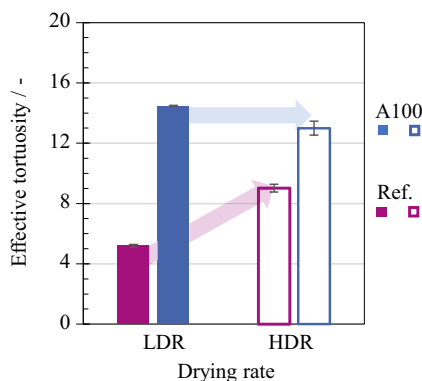


**Figure 8.** Effective tortuosity of electrodes made with the slurries Reference and A100 for the lower drying rate (LDR) of 0.75 g m<sup>-2</sup> s<sup>-1</sup> and the higher drying rate (HDR) of 6 g m<sup>-2</sup> s<sup>-1</sup>. The electrode structure is changed toward a higher effective tortuosity for A100, but adverse effects of a higher drying rate, like for the Reference, are not detected.

areas for diffusion by fully or partially blocked pores. On the other hand, the effective tortuosity for A100 remains at a higher value of around 13. A higher effective tortuosity fits to the generally worse, or equal C-rate capability of the anodes made with A100 compared to the anodes made with the Reference. It indicates that the transport of lithium ions to the graphite surface is aggravated either by longer diffusion pathways or by changes in the local microstructure. Comparing the slurries in the cryo-SEM images, the local arrangement of components is changed indeed (Figure 4) as well as the dry microstructure (Figure 3). The fact that the effective tortuosity does not change at increasing drying rate supports the hypothesis that less binder migration occurs for the anodes made with A100 unlike for the Reference.

The changed microstructure by use of the additive has ambivalent outcomes that must be utilized by further adaption of the processing: For A100, there is, from the performance perspective, no direct benefit for the use of this amount of the additive in a single layer. However, the concept of its use to mitigate binder migration may be combined with other approaches for microstructure optimization. The use in a multilayer with reduced binder content in the upper layer and additive in a functional layer will be investigated in future works.

### 3. Conclusion

In this work, the influence of the additive LAPONITE® on slurry properties, adhesion strength, and electrochemical performance was investigated for increasing drying rate. For the materials used, it could be confirmed that the additive usage transforms a liquid-like CMC solution into a gel-like dispersion. This influence could be transferred to water-based electrode slurries even for a reduction of all the passive materials and hence CMC, SBR, CB, and additive concentrations by up to 33%.

All the electrodes containing the additive showed a superior adhesion strength compared to a fast-dried Reference. For A100, A75, and the multilayer made with A100 near the current collector, an eight-time faster drying (30 s drying time for electrodes with 4.2 mAh cm<sup>-2</sup> areal capacity) could be realized without negative impact on adhesion due to binder migration.

However, changes in the compound network between the graphite in case of A100 are accompanied with an increased effective tortuosity and a worse C-rate capability compared to a slow-dried Reference. The effective tortuosity did not rise, and the C-rate capability was not adversely affected by increasing the drying rate from 0.75 to 6 g m<sup>-2</sup> s<sup>-1</sup>. Transferring this property to a multilayer electrode, further research in splitting the electrode in a thin bottom layer optimized for adhesion and electric connection, and a top layer optimized for electrochemical performance, offers new possibilities, because the characterization of a multilayer with the Reference in the top layer and A100 in the bottom layer via EDS did not indicate binder migration from out the bottom layer.

In summary, binder migration at increasing drying rate can be reduced using an additive but must be combined with optimization of either the formulation or, as the most promising approach, the use of structural optimization in a multilayer to be both beneficial for the electrodes adhesion and the performance of fast dried electrodes. The alterations in electrode

microstructure incorporating LAPONITE® are to be explored in future studies, along with the coating of multilayer electrodes, aiming to broaden the scope of microstructure optimization not only for lithium- but also for sodium-ion batteries.

## 4. Experimental Section

**Mixing of CMC–LAPONITE® Dispersion:** The investigated CMC solutions (Sunrose MAC500LC, Nippon Paper Industries, Japan) were made with a laboratory stirrer (Ø 42 mm) dissolver stirrer (IKA, Germany) in a beaker (800 mL). For the LAPONITE® dispersions, first LAPONITE® RD (BYK-Chemie GmbH, Germany) was dispersed in water (600 rpm, 10 min) until a bluish transparent dispersion was obtained. CMC was added under stirring and dissolved (600 rpm, 30–45 min) until a transparent solution was obtained.

**Slurry Mixing:** The slurries made with the graphite (SMGA, Hitachi Chemical Co. Ltd., Japan) were mixed in a dissolver (Dispermat SN-10, VMA Getzmann GmbH Verfahrenstechnik, Germany). First, CB (Super C65, Timcal SA, Switzerland) was dispersed in a 2 wt% CMC (Sunrose MAC500LC, Nippon Paper Industries, Japan) solution (1500 rpm, 30 min) containing the LAPONITE® already. The active material particles were added in three steps with short mixing steps (400 rpm, 1 min). Further water was added for the final solid content. The slurries were then dispersed further (1500 rpm, 30 min). In the final step, SBR (Zeon Europe GmbH, Japan) was added as dispersion in water (500 rpm, 10 min with degassing). The composition was chosen so that the dry electrode had the composition as shown in Table 1. The viscosity was measured by a rotational viscometer Physica MCR 101 (Anton Paar, Germany) with a plate–plate geometry (Ø25 mm, 0.01–1.000 s<sup>-1</sup> at 25 °C).

**Cryo-SEM Measurements:** The SEM images were taken from slurry samples frozen in a nitrogen slush. The slurry was coated as a droplet onto a metal foil and directly frozen. The preparation of a cross section of the slurry was done under liquid nitrogen using a diamond saw. The samples were transferred via a nitrogen-cooled shuttle (Leica VCT100) into a cryogenicbroad-ion-beam treatment (Leica TIC3X). Ion sputtering was conducted producing a smooth surface (3–4 h, 5 kV). The observation of the samples in a cryo-SEM (Zeiss Supra 55, equipped with an Oxford Instruments X-Max150 EDS detector) were conducted at 1 kV acceleration voltage for high-resolution micrographs and at 8 kV acceleration for electron images in combination with EDS, respectively, at a pressure of 2 E-005 mbar and a temperature of –140 °C. By heating up to –80 °C, the water was sublimated from the surface-near pores to get a view on the structure of the colloid system between the graphite particles.

**Electrode Coating and Drying:** The coating and drying of the graphite slurries was carried out in a discontinuous process as described by Baunach et al.<sup>[58]</sup> The 10 µm copper current collector (Civen Metal Material Co. Ltd., China) was attached to a temperature-controlled plate via suction. The coating of the anode slurries was applied with a doctor blade ZUA 2000.60 (Zehntner GmbH, Switzerland). In case of a simultaneous multilayer coating two doctor blades were joined. The coating gap of the bottom layer was adjusted assuming a proportional relationship between coating gap and wet film thickness. Subsequently, the coating was run under the drying nozzles of an impingement dryer under periodically movement. The drying rate was set by adjusting the temperature of the heated plate and drying gas while maintaining a constant heat-transfer coefficient of the slot nozzle dryer. The dew point of the air supplied was considered. **Table 2** shows the drying rates, the heat-transfer coefficients, and the drying temperature range. Further information on the drying setup is given in the literature.<sup>[2,4]</sup>

**Electrode Characterization:** The porosity was calculated from the areal mass loading divided by the layer thickness and the density of the dry mixture of the components. For the SEM/EDS of the electrode top, a field-emission SEM (Zeiss Supra 55) from Carl Zeiss AG (Oberkochen, Germany) was used.

**Table 2.** Overview of the drying rates and the drying temperatures with a constant heat-transfer coefficient of 35 W m<sup>-2</sup> K<sup>-1</sup>. The dew point for the experiments ranged from –1 to 14 °C. The drying temperature was set according to the dew point on the experiments' day.

Drying rate [g m <sup>-2</sup> s <sup>-1</sup> ]	Heat-transfer coefficient [W m <sup>-2</sup> K <sup>-1</sup> ]	Film temperature range [°C]
0.75	35	27.6–31.7
3	35	49.9–51.4
6	35	62.7–63.4

**Adhesion Strength:** To determine the adhesion strength, a 90° peel test was carried out with a universal testing machine AMETEK LS1 (Lloyd Instruments Ltd., UK) and a 10 N load cell. All samples of the dried anodes were cut out (width of 30 mm). The sample were fixated with coating side on an adhesive tape and pressed on by rolling once with a cylindrical weight (10 kg) to ensure uniform contact. The current collector foil was peeled off the coating at a constant speed (600 mm min<sup>-1</sup>) at a 90°-angle while measuring the peel strength.

**Cell Tests:** The anodes were electrochemically examined in pouch full cells (50 × 50 mm) against a NMC622 counter electrode. Foregoing the assembly of the cells, the electrodes were post-dried in a vacuum oven (110 °C, 16 h) to evaporate any residual water. The electrolyte used was LP30 (BASF) with the conductive salt 1M LiPF<sub>6</sub> in an ethylene carbonate (EC), dimethyl carbonate (DMC) mixture (EC/DMC=50/50, v/v). As separator S240P30 (SEPARION) was used.

The cycling was carried out in constant current mode inside a voltage range (3–4.3 V). Different C rates were used for charging and discharging. After two formation cycles at a C rate of C/20, the C rate was gradually increased up to 5 C. Then additional steps were carried out at C/2 and 1 C with a subsequent long-term cycling at 1C until the cells reached a total of 300 cycles.

**Impedance Spectroscopy:** The ionic resistance R<sub>ion</sub> was measured in symmetric coin cells (CR2032) with one spacer for each electrode and two glass fiber separators (GF/C, Whatman) per cell. As electrolyte tetrabutylammonium perchlorate (TBAClO<sub>4</sub>, 10 mM) in EC/DMC (50/50, v/v) was used (200 µL). It does not contain ions, that can be intercalated into the active material (blocking electrolyte). The conductivity of this electrolyte was κ = 0.3505 ± 0.0011 mS cm<sup>-1</sup>. Electrodes and separators were punched out with a diameter of 1.6 cm corresponding to an area A = 2.01 cm<sup>2</sup>. EIS measurements (10 mV perturbation, frequency range 200 kHz–100 mHz) were performed in a temperature-controlled chamber (BTZ-175, Espec) at 25 °C using a coin cell holder (Dual CR2032 Coin Cell Holder, Gamry Instruments) with a potentiostat (VSP-300, Biologic). For evaluation, the EIS software (RelaxIS 3, rhid instruments) was used using a transmission line model to obtain the ionic transport resistance R<sub>ion</sub>. The effective tortuosity was calculated by Equation (2) with the dry film thickness h<sub>dry</sub> and the porosity ε of the electrode after Landesfeind et al.<sup>[57]</sup>

$$\tau_{\text{eff}} = \frac{R_{\text{ion}} A \kappa \epsilon}{2 h_{\text{dry}}} \quad (2)$$

## Supporting Information

Supporting Information is available from the Wiley Online Library or from the author.

## Acknowledgements

This work contributes to the research performed at CELEST (Center for Electrochemical Energy Storage Ulm Karlsruhe) and Material Research

Center for Energy Systems (MZE). It was funded by the Deutsche Forschungsgemeinschaft (DFG, German Research Foundation) under Germany's Excellence Strategy—EXC 2154—project number: 390874152 (POLiS Cluster of Excellence). The authors would like to thank the assistants involved in this work especially Leonard Brilmayer and Max Buck who contributed to experimental results.

Open Access funding enabled and organized by Projekt DEAL.

## Conflict of Interest

The authors declare no conflict of interest.

## Data Availability Statement

The authors declare that the data supporting the findings of this study are available within the paper and the Supplementary Information file. Additional data and metadata, is available in the Zenodo repository with the DOI: <https://doi.org/10.5281/zenodo.10893349>.

## Keywords

binder migration, electrode processing, LAPONITE, lithium-ion batteries (LIBs), microstructure optimization, multilayer electrodes, slurry microstructure

Received: January 10, 2024

Revised: March 29, 2024

Published online:

- [1] J. Kumberg, W. Bauer, J. Schmatz, R. Diehm, M. Tönsmann, M. Müller, K. Ly, P. Scharfer, W. Schabel, *Energy Technol.* **2021**, 2100367.
- [2] J. Klemens, L. Schneider, E. C. Herbst, N. Bohn, M. Müller, W. Bauer, P. Scharfer, W. Schabel, *Energy Technol.* **2022**, 2100985.
- [3] S. Jaiser, M. Müller, M. Baunach, W. Bauer, P. Scharfer, W. Schabel, *J. Power Sources* **2016**, 318, 210.
- [4] J. Kumberg, M. Müller, R. Diehm, S. Spiegel, C. Wachsmann, W. Bauer, P. Scharfer, W. Schabel, *Energy Technol.* **2019**, 7, 1900722.
- [5] B. G. Westphal, H. Bockholt, T. Gunther, W. Haselrieder, A. Kwade, *ECS Trans.* **2015**, 64, 57.
- [6] R. Morasch, J. Landesfeind, B. Suthar, H. A. Gasteiger, *J. Electrochem. Soc.* **2018**, 165, A3459.
- [7] B. G. Westphal, A. Kwade, *J. Energy Storage* **2018**, 18, 509.
- [8] S. Jaiser, N. Sanchez Salach, M. Baunach, P. Scharfer, W. Schabel, *Dry. Technol.* **2017**, 35, 1807.
- [9] A. Altvater, T. Heckmann, J. C. Eser, S. Spiegel, P. Scharfer, W. Schabel, *Energy Technol.* **2022**, 2200785.
- [10] H. Luo, C. M. Cardinal, L. E. Scriven, L. F. Francis, *Langmuir* **2008**, 24, 5552.
- [11] P. Bernada, D. Bruneau, *Tappi J.* **1996**, 79, 130.
- [12] S. Jaiser, J. Kumberg, J. Klaver, J. L. Urai, W. Schabel, J. Schmatz, P. Scharfer, *J. Power Sources* **2017**, 345, 97.
- [13] S. Lim, K. H. Ahn, M. Yamamura, *Langmuir* **2013**, 29, 8233.
- [14] M. Weber, R. Moschner, A. Kwade, *Energy Technol.* **2022**, 2200852.
- [15] G. G. Eshetu, E. Figgemeier, *ChemSusChem* **2019**, 12, 2515.
- [16] J. Klemens, L. Schneider, D. Burger, N. Zimmerer, M. Müller, W. Bauer, H. Ehrenberg, P. Scharfer, W. Schabel, *Energy Technol.* **2023**, 2300338.
- [17] W. J. Chang, G. H. Lee, Y. J. Cheon, J. T. Kim, S. I. Lee, J. Kim, M. Kim, W. I. Park, Y. J. Lee, *ACS Appl. Mater. Interfaces* **2019**, 11, 41330.
- [18] C. Kugge, *J. Pulp Paper Sci.* **2004**, 30, 105.
- [19] J. C. Ese, B. Deichmann, T. Wirsching, L. Merklein, M. Müller, P. Scharfer, W. Schabel, *Dry. Technol.* **2020**, 1.
- [20] L. Gottschalk, J. Müller, A. Schoo, E. Baasch, A. Kwade, *Batteries* **2024**, 10, 40.
- [21] R. Diehm, J. Kumberg, C. Dörrer, M. Müller, W. Bauer, P. Scharfer, W. Schabel, *Energy Technol.* **2020**, 8, 1901251.
- [22] S. Lim, S. Kim, K. H. Ahn, S. J. Lee, *J. Power Sources* **2015**, 299, 221.
- [23] A. Benchabane, K. Bekkour, *Colloid Polym. Sci.* **2008**, 286, 1173.
- [24] G. Engström, I. Fineman, Persson A., I. Karlsson, R. Akesson, Trocknung von Stärkehaltigen Streichfarben. Erfahrungen mit der Trocknung in Schwebetrocknern, Biberach an der Riß, Wochenblatt für Papierfabrikation **1980**, 19, 793.
- [25] K. G. Hagen, *Tappi J.* **1986**, 93.
- [26] A. Heinzl, B. Capraro, B. Oberschachtsiek, Innovations Report IGF Forschungsvorhabensnummer 18437 BG, **2017**.
- [27] R. V. Hagen, R. Hoffmann, L. Klosowska, S. Nield, P. Jenness, J. Doyle, **2016**.
- [28] D. W. Thompson, J. T. Butterworth, *J. Colloid Interface Sci.* **1992**, 151, 236.
- [29] H. Z. Cummins, *J. Non-Cryst. Solids* **2007**, 353, 3891.
- [30] S. S. Das, K. Hussain, S. Singh, A. Hussain, A. Faruk, M. Tebyetekerwa, *Curr. Pharm. Des.*, 25, 424.
- [31] N. Willenbacher, *J. Colloid Interface Sci.* **1996**, 182, 501.
- [32] I. J. M. Corzo, J. H. L. Da Fonsêca, M. A. d'Ávila, *Rheol. Acta* **2023**, 62, 393.
- [33] P.-I. Au, S. Hassan, J. Liu, Y.-K. Leong, *Chem. Eng. Res. Des.* **2015**, 101, 65.
- [34] F. R. Fitch, P. K. Jenness, S. E. Rangus, in *Advances In Measurement and Control of Colloidal Processes* (Eds.: R. A. Williams, N. C. de Jaeger), Butterworth-Heinemann, Oxford **1991**, pp. 292–307.
- [35] *High Polymers* (Eds: E. Ott, N. Bikales), Vol. 5,5, Interscience Publ, New York, NY **1971**.
- [36] A. M. Zhivkov, in *Cellulose - Fundamental Aspects* (Ed.: T. G. van de Ven), InTech, London, England **2013**.
- [37] P. Xu, T. Erdem, E. Eiser, *Soft Matter* **2020**, 16, 5497.
- [38] K. Suman, Y. M. Joshi, *Langmuir* **2018**, 34, 13079.
- [39] A. Y. Malkin, S. R. Derkach, V. G. Kulichikhin, *Gels* **2023**, 9, 715.
- [40] *Das Rheologie-Handbuch. Für Anwender Von Rotations- Und Oszillations-Rheometern* (Eds: T. Mezger, U. Zorll), Vincentz, Hannover **2000**.
- [41] J. H. Park, S. H. Kim, K. H. Ahn, *Colloids Surf. A* **2023**, 664, 131130.
- [42] S. Spiegel, A. Hoffmann, J. Klemens, P. Scharfer, W. Schabel, *Energy Technol.* **2022**, 2200684.
- [43] H. H. Heimes, A. Kampker, C. Lienemann, M. Locke, C. Offermanns, S. Michaelis, E. Rahimzei, *Lithium-Ion Battery Cell Production Process*, PEM der RWTH Aachen University; DVMA, Aachen, Frankfurt am Main **2018**.
- [44] K. Hofmann, A. D. Hegde, X. Liu-Theato, R. Gordon, A. Smith, N. Willenbacher, *J. Power Sources* **2024**, 593, 233996.
- [45] A. Deirieh, I. Y. Chang, M. L. Whittaker, S. Weigand, D. Keane, J. Rix, J. T. Germaine, D. Joester, P. B. Flemings, *Appl. Clay Sci.* **2018**, 152, 166.
- [46] K. Park, M. Ryu, Y. Jung, H. E. Yoo, S. Myeong, D. Lee, S. C. Kim, C. Kim, J. Kim, J. Kwon, K. Lee, C.-W. Cho, U. Paik, T. Song, *Batteries Supercaps* **2023**, e202300170.
- [47] M. Alimardani, F. Abbassi-Sourki, *J. Compos. Mater.* **2015**, 49, 1267.
- [48] H. Yamamoto, H. Mori, in *Lithium-Ion Batteries* (Eds.: M. Yoshio, R. J. Brodd, A. Kozawa), Springer New York, New York, NY, **2009**, pp. 1–17.

- [49] J. A. SOLARIS, A. C. de Araujo, J. S. Laskowski, *Coal Prep.* **1986**, 3, 15.
- [50] M. Manilo, N. Lebovka, S. Barany, *Mater. Sci. Eng.* **2015**, 40, 96.
- [51] M. Park, X. Zhang, M. Chung, G. B. Less, A. M. Sastry, *J. Power Sources* **2010**, 195, 7904.
- [52] A. Pek-Ing, L. Yee-Kwong, *Appl. Clay Sci.* **2015**, 107, 36.
- [53] T. Wakamatsu, Y. Numata, *Miner. Eng.* **1991**, 4, 975.
- [54] C.-C. Wu, C.-C. Li, *ACS Sustainable Chem. Eng.* **2020**, 8, 6868.
- [55] F.-Y. Tsai, J.-H. Jhang, H.-W. Hsieh, C.-C. Li, *J. Power Sources* **2016**, 310, 47.
- [56] S. Jain, P. S. Sandhu, R. Malvi, B. Gupta, *J. Appl. Pharm. Sci.* **2013**, 3, 139.
- [57] J. Landesfeind, J. Hattendorff, A. Ehrl, W. A. Wall, H. A. Gasteiger, *J. Electrochem. Soc.* **2016**, 163, A1373.
- [58] M. Baunach, S. Jaiser, S. Schmelzle, H. Nirschl, P. Scharfer, W. Schabel, *Dry. Technol.* **2016**, 34, 462.